Joint Maximum Likelihood Estimation of Carrier Frequency Offset and Channel in Uplink OFDMA Systems

Man-On Pun†, Shang-Ho Tsai and C.-C. Jay Kuo
Department of Electrical Engineering and Signal and Image Processing Institute
University of Southern California, Los Angeles, CA 90089-2564, USA

Abstract— **A maximum likelihood estimator (MLE) that jointly estimates the carrier frequency offset (CFO) and the channel response of each user in uplink OFDMA systems is investigated in this research. The proposed MLE distinguishes itself from existing methods by its applicability to more flexible carrier assignment schemes. It achieves high computational efficiency by transforming a multidimensional optimization problem into a one-dimensional optimization problem. A suboptimal method is developed to further reduce the computational complexity. It is demonstrated by simulation results that the proposed MLE can provide accurate CFO and channel estimation in both SISO and SIMO environments.**

I. Introduction

Being effective in combating multipath mobile wireless channels, the Orthogonal Frequency Division Multiple Access (OFDMA) technology has attracted much attention recently as one of the most promising techniques for broadband wireless communications. An OFDMA system divides available carriers into groups, called subchannels, and assign one or multiple subchannels to multiple users. Two critical issues in the design of an uplink OFDMA system are investigated in this work. They are carrier frequency offset (CFO) estimation and channel estimation. Similar to OFDM, OFDMA is sensitive to the CFO between the transmitter and the receiver. Inaccurate CFO estimation results in the loss of orthogonality among carriers, thus leading to severe performance degradation. In addition, channel estimation for each user in the system is another indispensable task for achieving high-rate data transmission. These two tasks are especially challenging in uplink OFDMA because of the existence of multiple CFO's and transmission channels.

CFO estimation for uplink OFDMA has been studied by researchers, *e.g.* [1,2]. However, existing methods focus on either sub-band carrier assignment or interleaved carrier assignment. Consider that there are K users in the system. For sub-band carrier assignment, the system divides carriers into K consecutive subchannels and assigns each subchannel to one of the K users. For interleaved carrier assignment, carriers j, $K+j$, $2K+j$, $\cdots$ are assigned to user j, where $1 \le j \le K$. The recent trend of OFDMA favors a more flexible carrier assignment scheme. An example is given in Fig. 1 [3], where each user can select whatever carriers that are available at a particular time instance. Since there is no rigid association between carriers and users, the generalized carrier assignment scheme provides more flexibility than the sub-band and the interleaved schemes, when dynamic resource allocation or adaptive modulation is widely used in the near future.

The main contribution of this work is the proposal of a maximum likelihood estimator (MLE) that jointly estimates CFO and channel with low complexity. The proposed scheme demands that all users send one pilot FFT block in the time domain in the beginning of the uplink transmission process and, consequently, it is applicable to any subcarrier assignment schemes. Since a similar uplink transmission structure has been specified in IEEE802.16a (Fig.128av of [3]), this requirement should not be a serious constraint in practical OFDMA systems.

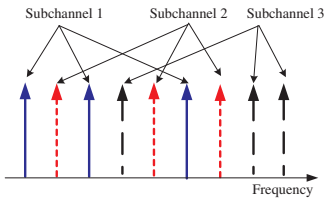

Fig. 1. Illustration of a generalized carrier assignment scheme.

II. Signal Models For OFDMA Uplink Transmissions

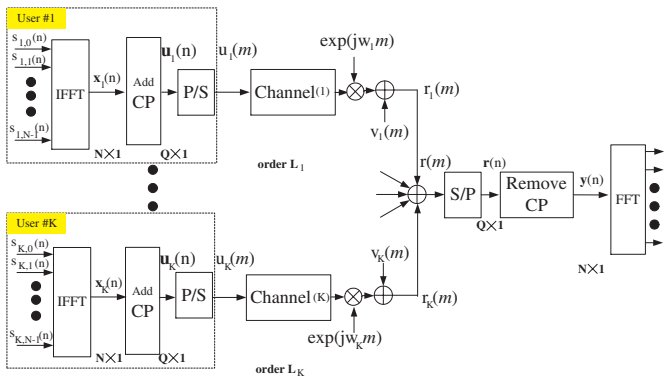

Fig. 2. OFDMA discrete-time equivalent baseband model

We consider the uplink of an OFDMA system employing N subcarriers as depicted in Fig. 2. The waveform arriving at the base station (BS) is given by the superposition of the signals from K active users. We denote $\boldsymbol{s}_k(n)$ the nth block of frequency-domain symbols sent by the kth user, where $k \in \{1, 2, \cdots, K\}$. The jth entry of $\boldsymbol{s}_k(n)$, say $s_{k,j}(n)$, is non-zero if and only if the jth carrier is assigned to the

†Author for all correspondence, mpun@usc.edu, telephone/fax (213)-748-7663.

kth user, with $j \in \{0, 1, \cdots, N-1\}$. The corresponding time-domain vector is given by

$$\boldsymbol{x}_k(n) = \boldsymbol{F}^H \boldsymbol{s}_k(n), \tag{1}$$

where $\boldsymbol{F}$ is the N-point discrete Fourier transform (DFT) matrix and $(\cdot)^H$ denotes Hermitian transposition. A cyclic prefix (CP) of length N_g is appended in front of $\boldsymbol{x}_k(n)$ to eliminate interblock interference (IBI). The resulting vector $\boldsymbol{u}_k(n)$ (with length $Q = N + N_g$) is transmitted over the channel. We denote $\{h_k(l)\}$ the kth user's discrete-time composite channel impulse response (including the shaping filters) of order L_k and define the corresponding channel response vector as

$$\boldsymbol{h}_k \stackrel{\text{def}}{=} [h_k(0), h_k(1), \cdots, h_k(L_k)]^T, \tag{2}$$

where $(\cdot)^T$ denotes the transpose operator.

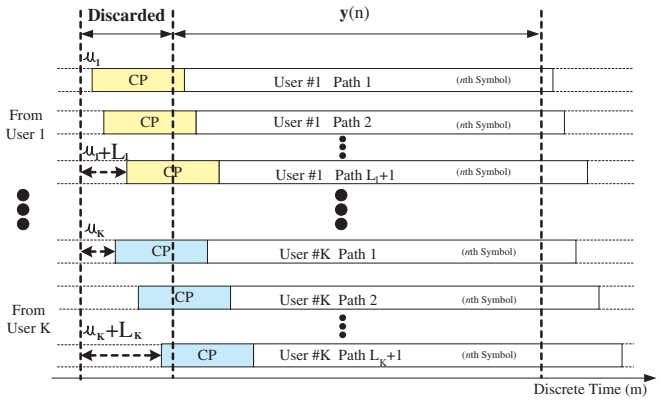

Fig. 3. Multipath and timing errors

In the presence of both CFOs and timing errors, the discrete-time output of the BS receive filter is given by

$$r(m) = \sum_{k=1}^{K} \left\{ e^{j\omega_k m} \sum_{l=0}^{L_k} h_k(l) u_k(m - l - \mu_k) \right\} + v(m), \tag{3}$$

where

- $\omega_k = \frac{2\pi \Delta f_k}{N}$, Δf_k being the kth CFO normalized to the subcarrier spacing;
- μ_k is the integer-valued timing error of the kth user as depicted in Fig. 3. As in [4], the fractional part of the timing error is incorporated into the channel impulse response;
- $v(m)$ is zero-mean white Gaussian noise with variance σ_v^2.

As shown in Fig. 2, at the BS the received samples $r(m)$ are serial-to-parallel (S/P) converted to form $\boldsymbol{r}(n)$. Next, the cyclic prefix is removed and the remaining samples are collected into the N-dimensional vector $\boldsymbol{y}(n)$. We consider a quasi-synchronous system in which the user timing is locked to a signal received from the BS through a downlink synchronization channel [4]. In this way the timing errors in the uplink are only due to the (two-way) line-of-sight propagation delay and are limited to $\mu_{\max} = 2R/c$, where R is the cell radius and c the speed of light. To proceed, we define $L_{\max} \stackrel{\text{def}}{=} \max_k \{\mu_k + L_k\}$ and assume that $N_g \geq L_{\max}$. This assumption is not restrictive as in practical applications the training blocks are preceded by long CPs. In these circumstances, we see that vector $\boldsymbol{y}(n)$ is not affected by IBI.

In the following , we assume that each user transmit pilot symbols over its pre-assigned subcarriers during the nth block (training block). Also, for notational simplicity, we omit the temporal index n in the sequel. Then, from Eq. (3), it turns out that $\boldsymbol{y}$ can be written in the following two equivalent matrix forms

$$\boldsymbol{y} = \sum_{k=1}^{K} e^{j\bar{\omega}_k} \boldsymbol{\Gamma}(\omega_k) \boldsymbol{A}_k \boldsymbol{\xi}_k + \boldsymbol{v}, \tag{4}$$

where

$$\boldsymbol{\Gamma}(\omega_k) = \text{diag}\left(1, e^{j\omega_k}, \cdots, e^{j(N-1)\omega_k}\right), \tag{5}$$

$$[\boldsymbol{A}_k]_{p,q} = [\boldsymbol{u}_k]_{p-q}, \qquad 1 \leq p \leq N, 1 \leq q \leq N_g + 1, \tag{6}$$

$$\boldsymbol{\xi}_k \stackrel{\text{def}}{=} \left[\begin{array}{ccc} \boldsymbol{0}^T_{\mu_k \times 1} & \boldsymbol{h}_k^T & \boldsymbol{0}^T_{(N_g - \mu_k - L_k) \times 1} \end{array} \right]^T, \tag{7}$$

and where

- $\bar{\omega}_k = \omega_k (nQ + N_g)$ is the phase associated with n;
- $[\boldsymbol{u}_k]_l$ is the lth entry of $\boldsymbol{u}_k$, with $-N_g + 1 \leq l \leq N - 1$.

In the following, the signal model of Eq. (4) is exploited to perform joint ML estimation of $\boldsymbol{\omega} = [\omega_1, \omega_2, \cdots, \omega_K]^T$ and $\boldsymbol{\xi} = \left[\boldsymbol{\xi}_1^T, \boldsymbol{\xi}_2^T, \cdots, \boldsymbol{\xi}_K^T\right]^T$. In this way, the estimation of the CFOs is decoupled from the estimation of $\boldsymbol{\xi}$ that embeds the timing error μ_k implicitly. Because of the specific structure of $\boldsymbol{\xi}_k$ given in Eq. (7), the timing error μ_k can be estimated as the index of the first significant element of $\hat{\boldsymbol{\xi}}_k$.

III. Joint Maximum Likelihood Estimation

A. Derivation of the ML Estimator

We begin by rewriting Eq. (4) into the following form

$$\boldsymbol{y} = \boldsymbol{Q}(\boldsymbol{\omega}) \boldsymbol{\xi} + \boldsymbol{v} \tag{8}$$

where

$$\boldsymbol{Q}(\boldsymbol{\omega}) = \left[\begin{array}{cccc} e^{j\bar{\omega}_1} \boldsymbol{\Gamma}(\omega_1) \boldsymbol{A}_1, & e^{j\bar{\omega}_2} \boldsymbol{\Gamma}(\omega_2) \boldsymbol{A}_2, & ..., & e^{j\bar{\omega}_K} \boldsymbol{\Gamma}(\omega_K) \boldsymbol{A}_K \end{array} \right] \tag{9}$$

Recalling that $\boldsymbol{v}$ is a vector of independent Gaussian random variables with zero-mean and variance σ_v^2, the joint ML estimation of $\boldsymbol{\omega}$ and $\boldsymbol{\xi}$ is given by

$$\left[\hat{\boldsymbol{\omega}}, \hat{\boldsymbol{\xi}}\right] = \arg\min_{\tilde{\boldsymbol{\omega}}, \tilde{\boldsymbol{\xi}}} \left\{ \left\| \boldsymbol{y} - \boldsymbol{Q}(\tilde{\boldsymbol{\omega}}) \tilde{\boldsymbol{\xi}} \right\|^2 \right\}, \tag{10}$$

where $\tilde{\boldsymbol{\omega}}$ and $\tilde{\boldsymbol{\xi}}$ are trial values of $\boldsymbol{\omega}$ and $\boldsymbol{\xi}$ respectively while $\|\boldsymbol{x}\|$ denotes the Euclidean norm of the enclosed vector $\boldsymbol{x}$.

To proceed further, we keep $\tilde{\boldsymbol{\omega}}$ fixed and minimize Eq. (10) with respect to $\tilde{\boldsymbol{\xi}}$. This produces

$$\hat{\boldsymbol{\xi}}\left(\tilde{\boldsymbol{\omega}}\right)=\left[\boldsymbol{Q}^{H}\left(\tilde{\boldsymbol{\omega}}\right)\boldsymbol{Q}\left(\tilde{\boldsymbol{\omega}}\right)\right]^{-1}\boldsymbol{Q}^{H}\left(\tilde{\boldsymbol{\omega}}\right)\boldsymbol{y} \tag{11}$$

Then, substituting Eq. (11) into Eq. (10) yields

$$\hat{\boldsymbol{\omega}}=\arg\max_{\tilde{\boldsymbol{\omega}}}\left\{\left\|\boldsymbol{P}_{\boldsymbol{Q}}\left(\tilde{\boldsymbol{\omega}}\right)\boldsymbol{y}\right\|^{2}\right\}, \tag{12}$$

where $\boldsymbol{P}_{\boldsymbol{Q}}\left(\tilde{\boldsymbol{\omega}}\right)=\boldsymbol{Q}\left(\tilde{\boldsymbol{\omega}}\right)\left[\boldsymbol{Q}^{H}\left(\tilde{\boldsymbol{\omega}}\right)\boldsymbol{Q}\left(\tilde{\boldsymbol{\omega}}\right)\right]^{-1}\boldsymbol{Q}^{H}\left(\tilde{\boldsymbol{\omega}}\right)$. Note that Eq. (12) can be interpreted as maximizing the projection of $\boldsymbol{y}$ onto the space spanned by the columns of $\boldsymbol{Q}\left(\tilde{\boldsymbol{\omega}}\right)$.

A necessary condition for the existence of $\left[\boldsymbol{Q}^{H}\left(\tilde{\boldsymbol{\omega}}\right)\boldsymbol{Q}\left(\tilde{\boldsymbol{\omega}}\right)\right]^{-1}$ in Eq. (11) is that $(N_g+1)K\leq N$. This constraint limits the maximum number of active users that the system can support for given N and N_g. Fortunately, this constraint is not a serious limitation in practice.

B. Iterative CFO estimation via alternating projection

The alternating projection algorithm is an iterative method for the solution of multidimensional optimization problems [5]. This technique is used here to reduce the K-dimensional optimization problem in Eq.(12) to a series of K one-dimensional problems. The resulting procedure consists of *cycles* and *steps*. A cycle is made of K steps and each step updates the CFO of a single user while keeping the other CFOs constant and at their most updated values. Without loss of generality, we assume the user update order is $k=1,2,\cdots,K$. We denote $\hat{\omega}_k^{(i)}$ the estimate of ω_k at the ith cycle and define the $(K-1)$-dimensional vector $\hat{\boldsymbol{\omega}}_k^{(i)}$ as

$$\hat{\boldsymbol{\omega}}_k^{(i)}\stackrel{\text{def}}{=}\left[\hat{\omega}_1^{(i+1)},\cdots,\hat{\omega}_{k-1}^{(i+1)},\hat{\omega}_{k+1}^{(i)}\cdots,\hat{\omega}_K^{(i)}\right]^{T}. \tag{13}$$

Then, at the kth step of the ith cycle the alternating projection method updates the estimate of ω_k by solving the following 1D maximization problem

$$\hat{\omega}_k^{(i+1)}=\arg\max_{\tilde{\omega}_k}\left\{\left\|\boldsymbol{P}_{\boldsymbol{Q}}\left(\tilde{\omega}_k,\hat{\boldsymbol{\omega}}_k^{(i)}\right)\boldsymbol{y}\right\|^{2}\right\}. \tag{14}$$

where the notation $\boldsymbol{P}_{\boldsymbol{Q}}\left(\tilde{\omega}_k,\hat{\boldsymbol{\omega}}_k^{(i)}\right)$ has been used to indicate the functional dependence of $\boldsymbol{P}_{\boldsymbol{Q}}$ on $\left[\hat{\omega}_1^{(i+1)},\cdots,\hat{\omega}_{k-1}^{(i+1)},\tilde{\omega}_k,\hat{\omega}_{k+1}^{(i)}\cdots,\hat{\omega}_K^{(i)}\right]^{T}$. The ith cycle ends with the updating of $\hat{\omega}_K^{(i)}$. Next, we move to the $(i+1)$th cycle where $\hat{\boldsymbol{\omega}}_k^{(i+1)}$ $(k=1,2,\cdots,K)$ is employed to compute $\hat{\omega}_k^{(i+2)}$. Multiple cycles will be performed until the solution converges. Since the method increases the likelihood along a line parallel to each ω_k axis at each step, it is bounded to converge. Even though it is possible that the solution converges to a local maximum depending on the particular initialization [5], in all our experiments the method did converge to the true CFOs in a few cycles.

The maximization process discussed above involves an exhaustive grid search over the possible range of ω_k. However, evaluation of the likelihood function for each trial value of ω_k requires computing $\boldsymbol{P}_{\boldsymbol{Q}}\left(\tilde{\omega}_k,\hat{\boldsymbol{\omega}}_k^{(i)}\right)$, which involves a matrix inversion of dimension $K(N_g+1)\times K(N_g+1)$. Since most columns in $\boldsymbol{Q}\left(\tilde{\omega}_k,\hat{\boldsymbol{\omega}}_k^{(i)}\right)$ are fixed while optimizing a specific ω_k, we can avoid the huge matrix inversion by splitting $\boldsymbol{Q}\left(\tilde{\omega}_k,\hat{\boldsymbol{\omega}}_k^{(i)}\right)$ into two parts: $\boldsymbol{C}(\tilde{\omega}_k)$ containing all columns related to $\tilde{\omega}_k$ and $\boldsymbol{B}(\hat{\boldsymbol{\omega}}_k^{(i)})$ containing all columns *not* related to $\tilde{\omega}_k$. Eq. (15) gives an example for $k=1$.

$$\boldsymbol{Q}\left(\tilde{\omega}_1,\hat{\boldsymbol{\omega}}_1^{(i)}\right)=\Bigg[\underbrace{e^{j\tilde{\omega}_1}\boldsymbol{\Gamma}(\tilde{\omega}_1)\boldsymbol{A}_1}_{\boldsymbol{C}(\tilde{\omega}_1)},\ \underbrace{e^{j\hat{\omega}_2^{(i)}}\boldsymbol{\Gamma}(\hat{\omega}_2^{(i)})\boldsymbol{A}_2,\cdots,e^{j\hat{\omega}_K^{(i)}}\boldsymbol{\Gamma}(\hat{\omega}_K^{(i)})\boldsymbol{A}_K}_{\boldsymbol{B}(\hat{\boldsymbol{\omega}}_1^{(i)})}\Bigg] \tag{15}$$

Thus, we can decompose the projection $\boldsymbol{P}_{\boldsymbol{Q}}\left(\tilde{\omega}_k,\hat{\boldsymbol{\omega}}_k^{(i)}\right)$ into two parts: 1) $\boldsymbol{P}_{\boldsymbol{B}}$: projection onto the column space of $\boldsymbol{B}$ and 2) $\boldsymbol{P}_{\boldsymbol{C}_{\boldsymbol{B}}}$: the residual projection in the column space of $\boldsymbol{C}$ but *not* in the column space of $\boldsymbol{B}$. The idea behind this decomposition is similar to the Gram-Schmidt procedure and it is mathematically formulated as

$$\boldsymbol{P}_{\boldsymbol{Q}}\left(\tilde{\omega}_k,\hat{\boldsymbol{\omega}}_k^{(i)}\right)=\boldsymbol{P}_{\boldsymbol{B}}\left(\hat{\boldsymbol{\omega}}_k^{(i)}\right)+\boldsymbol{P}_{\boldsymbol{C}_{\boldsymbol{B}}}\left(\tilde{\omega}_k,\hat{\boldsymbol{\omega}}_k^{(i)}\right), \tag{16}$$

where $\boldsymbol{P}_{\boldsymbol{B}}=\boldsymbol{B}\left[\boldsymbol{B}^{H}\boldsymbol{B}\right]^{-1}\boldsymbol{B}^{H}$, $\boldsymbol{C}_{\boldsymbol{B}}=\left[\boldsymbol{I}_N-\boldsymbol{P}_{\boldsymbol{B}}\right]\boldsymbol{C}$ and $\boldsymbol{P}_{\boldsymbol{C}_{\boldsymbol{B}}}=\boldsymbol{C}_{\boldsymbol{B}}\left[\boldsymbol{C}_{\boldsymbol{B}}^{H}\boldsymbol{C}_{\boldsymbol{B}}\right]^{-1}\boldsymbol{C}_{\boldsymbol{B}}^{H}$.

As $\boldsymbol{P}_{\boldsymbol{B}}\left(\hat{\boldsymbol{\omega}}_k^{(i)}\right)$ is independent of $\tilde{\omega}_k$, Eq. (14) reduces to

$$\hat{\omega}_k^{(i+1)}=\arg\max_{\tilde{\omega}_k}\left\{\left\|\boldsymbol{P}_{\boldsymbol{C}_{\boldsymbol{B}}}\left(\tilde{\omega}_k,\hat{\boldsymbol{\omega}}_k^{(i)}\right)\boldsymbol{y}\right\|^{2}\right\}. \tag{17}$$

Note that computing $\boldsymbol{P}_{\boldsymbol{C}_{\boldsymbol{B}}}$ requires a significantly smaller matrix inversion than $\boldsymbol{P}_{\boldsymbol{Q}}$. In the sequel, the estimator in Eq. (17) is referred to as the Alternating-Projection Frequency Estimator (APFE).

C. Initialization of the CFOs estimates

Intuitively, the iterative procedure discussed previously has a higher chance to converge to the global maximum of the likelihood function if accurate estimates $\hat{\boldsymbol{\omega}}^{(0)}$ are used for initialization purposes. Two strategies are proposed to compute $\hat{\boldsymbol{\omega}}^{(0)}$. In the first strategy, $\hat{\omega}_k^{(0)}$ is simply initialized to its expected value, i.e. $\hat{\omega}_k^{(0)}=0$ (ω_k is modeled as a zero-mean random variable with uniform distribution). In the second strategy, $\hat{\omega}_k^{(0)}$ is taken as the output of the frequency estimator proposed in [6]. Note that the scheme in [6] was originally developed for single-user systems and, accordingly, it is not resistant to multiple access interference (MAI). However, simulations indicate that it provides a better initialization and a faster convergence rate than simply setting $\hat{\omega}_k^{(0)}=0$.

D. Algorithm Summary

Initialization: Initialize $\hat{\boldsymbol{\omega}}^{(0)}$.
Solving $\boldsymbol{\omega}$: Let $i = 0$
(1) For $k = 1, 2, \cdots, K$, compute $\hat{\omega}_k^{(i+1)}$ according to Eq. (17) using $\hat{\boldsymbol{\omega}}_k^{(i)}$ as defined in Eq. (13);
(2) Repeat (1) and update $i = i + 1$ until the stopping criterion is reached. A simple stopping criterion is to terminate after a preset number of cycles.

E. Suboptimal Method

In evaluating Eq.(17), we still have to perform an $(N_g + 1) \times (N_g + 1)$ matrix inversion for each possible value of $\tilde{\omega}_k$. Noticing that $\boldsymbol{C}^H(\tilde{\omega}_k)\boldsymbol{C}(\tilde{\omega}_k) = \boldsymbol{A}_k^H \boldsymbol{A}_k$ is independent of $\tilde{\omega}_k$, we can approximate the likelihood function using the von Neumann series [7]:

$$\left\|\boldsymbol{P}_{\boldsymbol{C}_{\boldsymbol{B}}}\boldsymbol{y}\right\|^2 \approx \boldsymbol{y}^H \boldsymbol{C}_{\boldsymbol{B}} \left[\sum_{p=0}^{P} (\boldsymbol{E})^p\right] \left(\boldsymbol{C}^H\boldsymbol{C}\right)^{-1} \boldsymbol{C}_{\boldsymbol{B}}^H \boldsymbol{y}, \quad (18)$$

where M is the approximation order and $\boldsymbol{E} = (\boldsymbol{C}^H\boldsymbol{C})^{-1}\boldsymbol{C}^H\boldsymbol{P}_{\boldsymbol{B}}\boldsymbol{C}$. It can be shown that all the eigenvalues of $\boldsymbol{E}$ have magnitude less than unity. Note that computing the right-hand-side (RHS) of Eq. (18) requires the inversion of $\boldsymbol{C}^H\boldsymbol{C}$, which is independent of $\tilde{\omega}_k$. Accordingly, we need only one matrix inversion for each user at each cycle. In the following, the estimator based on the approximation Eq. (18) is called the Approximate APFE (AAPFE).

F. Spatial Diversity

Using Q_r receive antennas, the BS can exploit the space diversity. Repeating the steps discussed previously, we can easily get the update function corresponding to Eq. (17) as

$$\hat{\omega}_k^{(i+1)} = \arg\max_{\tilde{\omega}_k} \left\{ \sum_{m=1}^{M} \left\| \boldsymbol{P}_{\boldsymbol{C}_{\boldsymbol{B}}} \left(\tilde{\omega}_k, \hat{\boldsymbol{\omega}}_k^{(i)}\right) \boldsymbol{y}_m \right\|^2 \right\}, \quad (19)$$

where $\boldsymbol{y}_m$ is the received block by the mth antenna.

IV. Simulation Results

In this section, we compare the performance of the proposed MLE and the suboptimal estimator previously proposed with the Cramer-Rao bound (CRB). [1] Without loss of generality, only the results for user#1 are illustrated in the sequel. Also, to evaluate the simulation results with reference to [8], we use the normalized frequency, Δf_k, in this section instead of the normalized angular frequency, ω_k, where $\omega_k = \frac{2\pi\Delta f_k}{N}$.

A. System Parameters

We consider an OFDMA system with $N = 128$ subcarriers in the 5 GHz frequency band. The signal bandwidth is 20 MHz, corresponding to an inter-carrier spacing of 156.25 kHz. The channel response of each user is generated according to the HIPERLAN/2 channel model with eight paths ($L_k = 7$). The channel coefficients are modeled as independent and complex-valued Gaussian random variables with zero-mean and an exponential power delay profile

$$E\left\{|h_k(l)|^2\right\} = \lambda_k \cdot \exp\{-l/2\}, \quad n = 0, 1, \cdots, 7. \quad (20)$$

The constant λ_1 is chosen such that the signal power of user#1 is normalized to unity, i.e., $E\left\{\|\boldsymbol{A}_1\boldsymbol{\xi}_1\|^2/Q\right\} = 1$. This means that the average SNR is equal to $1/\sigma_v^2$, where σ_v^2 is the variance of the Gaussian noise. Parameters λ_k (with $k \geq 2$) affect the signal-to-interference ratio and their values are specified in the various experiments.

We assume an overall instability of the transmitter/receiver oscillators of 10 ppm, corresponding to maximum CFO of 50 kHz. This is tantamount to setting $|\Delta f| \leq 0.32$, where Δf is the frequency offset normalized to the inter-carrier spacing.

The cell radius is 150 m, so that the (two-way) maximum propagation delay is $2R/c = 1\mu s$. Bearing in mind that the sampling periods is $T_s = 1/B = 5 \cdot 10^{-2}\mu s$, this makes the maximum of μ equal to 20. The training blocks have a CP of length $N_g = 30$ so as to accommodate both the channel response duration and the maximum propagation delay.

B. Example 1: resistance to near-far effects

In this experiment we assume that two users are active in the system ($K = 2$) with the signal power of the interfering user is 3dB higher than that of user#1 (this is achieved by setting $\lambda_2 = 2\lambda_1$ in Eq. (20)). 20 distinct subcarriers are randomly assigned to each of them. The AAPFE uses a first-order approximation, i.e., we set $M = 1$ in Eq. (18).

Fig. 4 shows the MSE of the frequency estimates vs. SNR as obtained with APFE and AAPFE. It turns out that the performance of APFE is only marginally affected by the near-far effect while a larger degradation occurs with AAPFE. However, extensive simulations (not shown in Fig. 4) indicate that the accuracy of AAPFE improves as M increases and approaches that of APFE for $M \geq 4$. The performance of the frequency synchronizer proposed by Morelli and Mengali (MMFE) in [6] are also shown for comparison. Because MMFE is designed for single-user systems and, accordingly, it performs poorly in the presence of MAI. As discussed in [8], the performance loss due to frequency errors are expected to be negligible when the MSE of the normalized CFO is on the order of $4 \cdot 10^{-4}$. Inspection of Fig. 4 reveals that both APFE and AAPFE meet this requirement for SNR values greater than 10 dB.

Fig. 5 shows the convergence behaviors of the MLE. In this example, the iteration process quickly converges after 3 iterations.

C. Example 2 :effect of K on the performance of the frequency estimators

Finally, we show the impact of the number of users, K, on the frequency estimation accuracy of the proposed

[1] Due to the limitation of space, we leave the derivation of CRB for future publication.

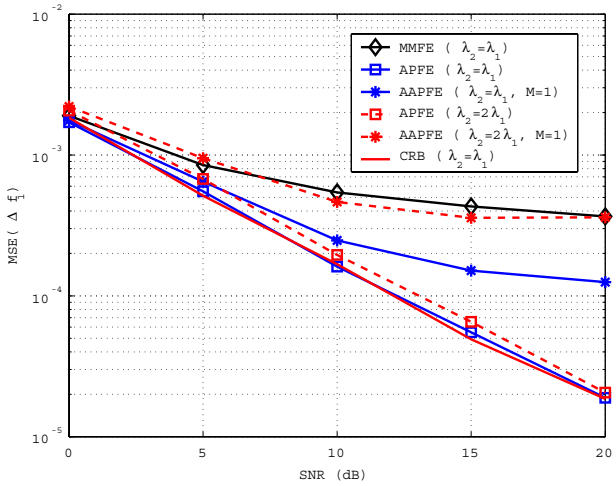

Fig. 4. Robustness against the Near-Far Effect

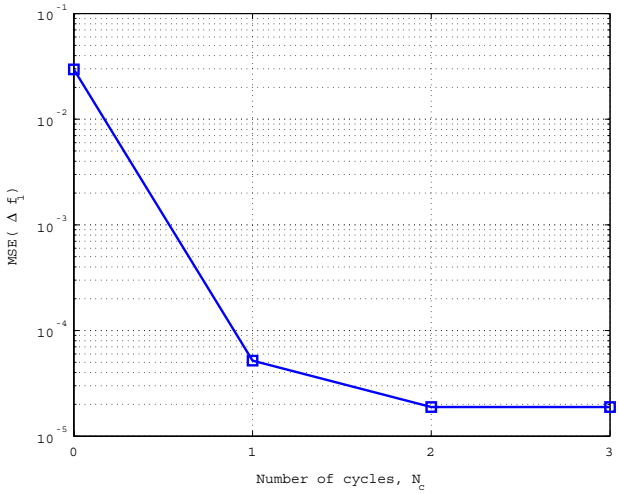

Fig. 5. Convergence behavior of CFO MLE

APFE. In particular, we consider the following three different cases: $N = 128$ with $K = 2, 3, 4$. In all cases, the users have the same power, i.e., $\lambda_k = \lambda_1$ for $k \geq 2$. As K increases, the amount of MAI increases. As a result, the performance of APFE decreases.

V. Conclusion

A maximum likelihood estimator (MLE) capable of jointly estimating CFO and channel for each user in uplink OFDMA was presented in this work. The proposed algorithm is attractive owing to its low computational complexity and general applicability to flexible subcarrier assignment schemes. The effectiveness of the proposed MLE is confirmed by computer simulation results.

VI. Acknowledgement

The authors would like to thank Dr. Michele Morelli of University of Pisa, Italy for the insightful discussion to improve this manuscript.

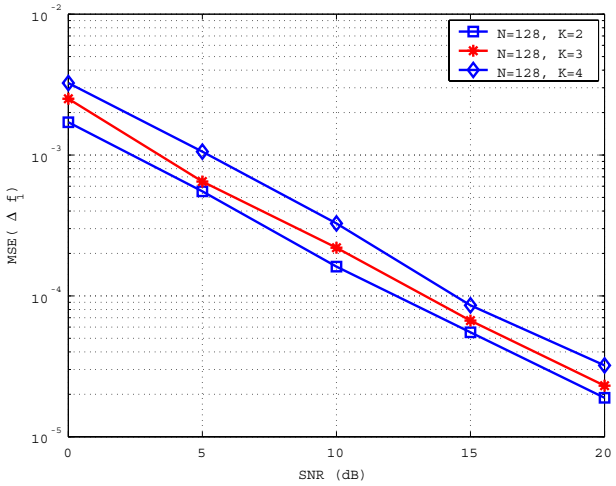

Fig. 6. Effect of K

References

[1] Z. Cao, U. Tureli, and Y. D. Yao, "Efficient structure-based carrier frequency offset estimation for interleaved ofdma uplink", *proceedings of ICC 2003*, 2003.

[2] S. Barbarossa, M. Pompili, and G.B. Giannakis, "Channel-independent synchronization of orthogonal frequency division multiple access systems", *IEEE JSAC*, vol. 20, no. 2, Feb 2002.

[3] *IEEE Standard for Local and metropolitan area networks - Part 16: Air Interface for Fixed Broadband Wireless Access Systems-Amendment 2: Medium Access Control Modifications and Additional Physical Layer Specifications for 2-11 GHz*, IEEE Std. 802.16a, 2003.

[4] M. Morelli, "Timing and frequency synchronization for the uplink of an ofdma system", *IEEE Trans. Communincations*, vol. 52, no. 2, February 2004.

[5] I. Ziskind and M. Wax, "Maximum likelohood localization of multiple sources by alternating projection", *IEEE Trans. Acoust. Speech, Signal Processing*, vol. 36, no. 10, Oct. 1988.

[6] M. Morelli and U. Mengali, "Carrier-frequency estimation for transmissions over selective channels", *IEEE Trans. Communincations*, vol. 48, no. 9, September 2000.

[7] D. Kincaid and W. Cheney, *Mathematics of Scientific Computing*, Brooks/Cole, second edition, 1996.

[8] P.H. Moose, "A technique for orthogonal frequency division multiplexing frequency offset correction", *IEEE Trans. Communincations*, vol. 42, no. 10, October 1994.